7-2015

Wing Tip Vortices from an Exergy-Based Perspective

Muhammad Omar Memon
University of Dayton, mmemon1@udayton.edu

Kevin Wabick
University of Dayton, wabickk1@udayton.edu

Aaron Altman
University of Dayton, aaltman1@udayton.edu

Rainer M. Buffo
RWTH Aachen University

Wingtip Vortices from an Exergy-Based Perspective

Muhammad Omar Memon[1], Kevin Wabick[2], Aaron Altman[3]
Department of Mechanical and Aerospace Engineering, University of Dayton, Dayton, OH 45469, USA

R.M. Buffo[4]
Research Engineer, Dipl.-Ing., Institute of Aerospace Systems (ILR), RWTH Aachen University, Wuellnerstrasse 7, 52062 Aachen, Germany

The lens of exergy is used to investigate a wingtip vortex in the near wake over a range of angles of attack. Exergy is the measure of thermodynamically "available" energy as determined through the more discriminating second law of thermodynamics. Experiments were conducted in a water tunnel at ILR Aachen. The data was taken three chord lengths downstream in the Trefftz plane of an aspect ratio (AR) 5 Clark-Y wing with a square edged wingtip using Particle Image Velocimetry (PIV). Intuitively, the minimum available energy state is expected to correspond to the maximum lift to drag ratio angle of attack. This, however, is not the case here. Most interestingly, although only 2-d Trefftz plane data was used to obtain the exergy distribution across the individual wingtip vortices, the crossover point for the *out of plane* change from wake-like to jet-like wingtip vortex core axial flow (indicating the peak lift to drag ratio) is identified by the *in-plane* exergy distribution. This crossover point is not identifiable in the evaluation of any other characteristics calculated from in-plane quantities. Consequently, the exergy method holds promise as a metric for the improvement of aircraft performance through the reduction of lift induced drag.

I. Introduction

Every aircraft designer aspires to maximize aircraft aerodynamic performance. Exergy-based approaches for aircraft design and integration have begun to attract some interest in an effort to achieve even higher efficiency. The term 'exergy' can be defined as the potential work that *could* be achieved from any given system. With lightweight and aerodynamically efficient structures, the most efficient designs could be obtained by minimizing the total exergy

[1] Ph.D. Candidate, Aerospace Engineering, mmemon1@udayton.edu
[2] M.S. Aerospace Engineering, kevin.wabick@gmail.com
[3] Associate Professor; Director, Graduate Aerospace Program, aaltman1@udayton.edu
[4] Research Engineer, Dipl.-Ing., buffo@ilr.rwth-aachen.de

destruction of the system. This destruction of exergy is proportional to the corresponding entropy generation [1]. A number of analytical methods have been used by researchers to perform exergy based analysis.

Exergy analysis could be applied to the aerodynamics of the wing to identify the maximum capability of the energy system in problems associated with wingtip vortices. The wingtip vortices develop by the pressure difference on the upper and lower surfaces of the wing as a byproduct of the way the aircraft produces lift [2]. The vortex system in the near wake is far more complex since strong vortices tend to continue developing in the near regions. The strength of these vortices is proportional to the total circulation [3]. Alabi et al. [1] compared empirical and CFD based exergy calculation procedures for modeling the airframe subsystem of an aircraft (B747-200). The exergy-based approach supported the viability of using CFD for realistic airframe calculations in a system-level analysis and design optimization. Various researchers [4-6] have applied exergy-based methods to aerodynamic problems. Li et al. [4] investigated the impact of exergy on aerodynamic designs by applying exergy-based methods to various two-dimensional airfoils and three-dimensional wings under turbulent flow conditions. The authors performed exergy-based optimization to minimize entropy for the airfoils under test. They found that the results from the 'exergy-based method' were in much better agreement with the semi-empirical value than the 'surface integration method' of obtaining drag values [4]. In addition, the exergy-based method resulted in a greater lift/drag ratio and less exergy destruction in comparison to the conventional method. Figliola and Tipton [6] compared the application of a traditional energy-based approach versus the exergy-based approach to the design of the environmental control system (ECS) of an advanced aircraft. The objective of the research was to minimize the gross takeoff weight by the applied design approaches. The authors concluded that the results from the two analyses provide solutions that are similar although not exactly the same. However, the exergy-based method provides a ready estimate for efficiency on a component and system basis [6].

The lift to drag ratio plays a vital role in aerodynamic systems and is closely related to the vortex formation. Lee and Pereira [7] tested square and round tips to investigate the mechanisms responsible for the wake-like and jet-like axial flows of a tip vortex. For smaller angles of attack, this pocket of jet-like fluid was entrained by the shear layers and the wing wake. For higher angles of attack, the jet-like fluid pocket was surrounded by the shear layers. The idea of the attainment of maximum lift to drag ratio corresponding to a transition in the vortex core axial flow from wake-like to jet-like will be investigated further through the perspective of exergy and reveals some interesting behavior.

Additionally, when applying the exergy-based perspective to the wingtip vortex problem, it is hypothesized that the minimum exergy destruction of the system would be obtained under the conditions where the lift to drag ratio is maximum. In this paper, the exergy of the wingtip vortex in the near wake is calculated from experimental data as a function of angle of attack from Trefftz plane PIV derived velocity field data. The experiments are conducted in a circular water tunnel at the ILR Aachen. The data are acquired three chord lengths downstream of a Clark-Y wing of aspect ratio 5 with a square edged wingtip.

II. Experimental Setup

The experiments are conducted in an enclosed circulating water tunnel with a test section of 1000 *mm* x 540 *mm* x 540 *mm* at the ILR Aachen in Germany [8]. The tunnel contraction ratio is 1/1.8 and the freestream velocity (U_∞) has a continuous range from 0 to 4 *m/s*. Figure 1 provides a schematic of the water tunnel. A constant Reynolds number of 200,000 is maintained throughout the tests cited in the present study. The freestream velocity was adjusted to account for kinematic viscosity variations due to rising water temperature while carrying out the measurements. The temperature variation across a given run was in the tenths of degrees Celsius as shown in Table 1. This small variation had negligible (2-3 orders of magnitude smaller) effect on the absolute entropy and hence the effects of the miniscule temperature changes were neglected.

Table 1 Temperature variations for various time steps during a representative run. Also showing min, max, mean and the temperature ratio.

Time Step	T (°C)
1	26.1
2	26.1
3	26.3
4	26.4
5	26.5
6	26.6
7	26.8
T min (°C)	26.1
T max (°C)	26.8
T mean (°C)	26.4
T diff min-max (°C)	0.7
T diff ratio to mean	2.65%

All measurements were performed at freestream velocities ranging between 2.2 and 2.5 *m/s*. The measurements used in the current paper represent the *x/c* = 3 plane downstream. Vortex core axial velocity is referenced to the freestream value $U_{\infty,}$ which is gathered in separate measurements in undisturbed flow. A function *f(rpm)*= U_{∞} is obtained, which delivers the freestream value for post processing the data.

Two CCD cameras were used to view the suction side of the wingtip where the primary and secondary vortices were expected to form. Water filled containers were positioned between the test section's glass windows and the cameras to avoid the optical refraction resulting from viewing across several refractive indices at an angle not normal to the image plane. The wing comprising a Clark-Y airfoil was mounted vertically from the ceiling of the test-section. It is important to note that all data included here was obtained for a cross-stream plane three chords length downstream. The wake was determined to be fully rolled up at this downstream location in Buffo et al. [9]. At 15° angle of attack, flow over the wing is expected to be separated. When following the core circulation across the complete range of angles of attack the trend is linear since the local core creation mechanism at the side edge is not affected by local separation in the wing-root area. At x/c = 3 at very high angles of attack most of the vorticity is already rolled up and in the field of view. Therefore also the trend of maximum circulation should allow for assessing how much flow is still attached. Theoretical maximum circulation may also be calculated when assuming elliptic lift distribution which is reasonable at AR = 5.

The laser beam was expanded to a light-sheet of 2 mm thickness. In order to minimize systematic errors, a small aperture of f = 8 provided a minimum depth of focus with a maximum light-sheet spread-angle and minimum operational laser power. Every series was recorded with 500 image pairs at 1 Hz recording frequency and an interframe delay ranging from 100 − 117 μs. Using objectives with a focal length of 100 mm the size of the viewing area was 55 mm x 70 mm and was divided into correlation windows of 32 x 32 pixels with an overlap of 75%. This yielded an overall resolution of 17 vectors per mm. The blockage ratio at 10° angle of attack was 0.95% with a turbulence intensity of 2.5%. The turbulence intensity results from a very modest water tunnel inlet contraction ratio of 1.8.

To account for vortex wandering, a method for aligning the single vorticity fields according to a common overall vortex center is implemented. This method provides velocity profiles which are not stretched and do not suffer from diminished peaks. As opposed to the vortex development phase in the near-wake behind a wing, the path

of the center of the azimuthal velocity field (vortex center) during the vortex creation phase at the wing-tip is highly 3-dimensional. The vortex spirals around the tip and the axis and thus the axial and azimuthal (circulation) field permanently change their orientation. Therefore the velocity fields undergo an Euler transformation according to the angle of the predetermined vortex axis. Figure 2 shows the corresponding coordinate axis definition [8]. It is noteworthy that the y and z axes define the cross-plane in the experiments where the x-axis represents the out of plane component.

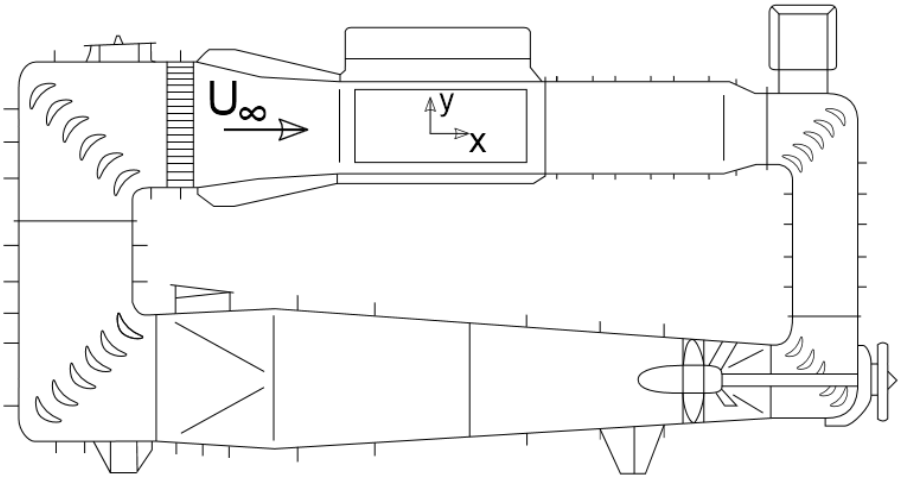

Fig. 1 Circulating water tunnel at ILR, RWTH Aachen University, with the coordinate system definition

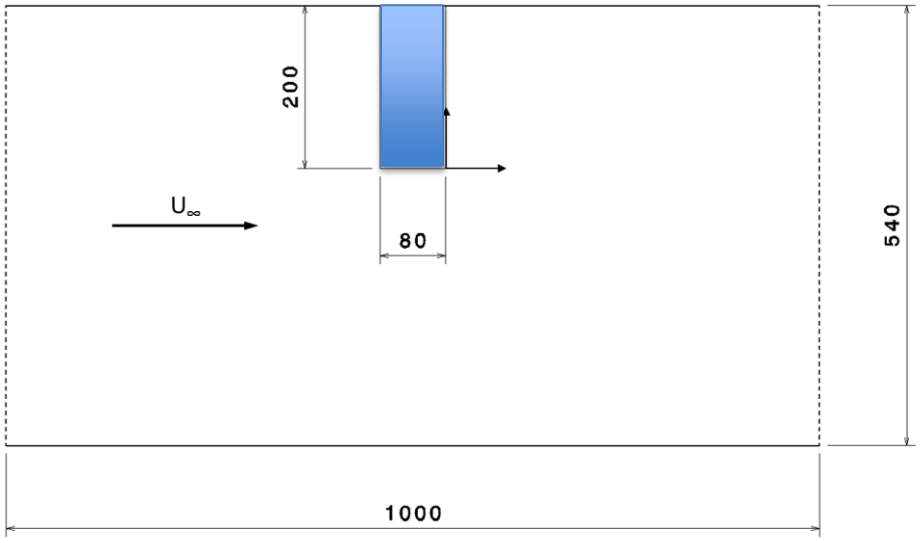

Fig. 2 Schematic of the test section with half wing installed. All dimensional units are in millimeters (mm).

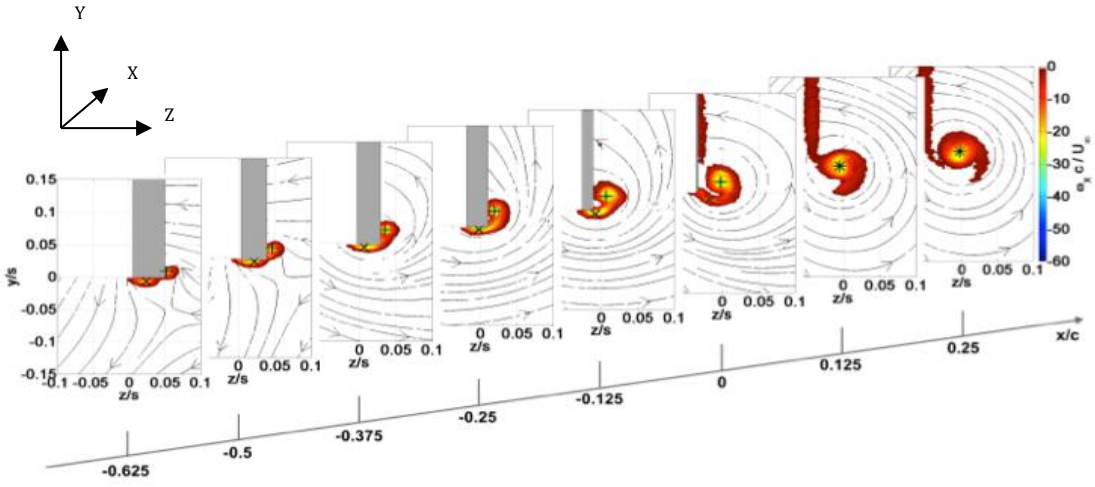

Fig. 3 Representation of the axial vorticity during the vortex creation at the wingtip [9]

III. Background Theory

Traditionally exergy is used to describe performance of thermal systems however there is tremendous potential in fluid systems too. Analyzing the wingtip vortex from the entropy generation standpoint reveals an alternate possibile manner to optimize the system. Thus, using this approach the viscous dissipation rate can be quantified by the entropy generation involved in the process [10], which is considered as work potential within the system. In other words, work potential is directly related to the exergy destruction rate. The exergy destruction rate can be used as an objective parameter to improve any system in its capacity to quantify the losses.

According to the second law of thermodynamics, only a portion of energy at a temperature above the environment temperature can be converted into work. The maximum useful work is produced by passing energy transfer through a reversible system. Expressing this concept through the laws of thermodynamics, the first law of thermodynamics can be written as,

$$E_{in} - E_{out} = \dot{E}_{sys} \tag{1}$$

The second law of thermodynamics is expressed as

$$\dot{S}_{in} - \dot{S}_{out} + \dot{S}_{gen} = \dot{S}_{sys} \quad (2)$$

Where $\dot{S}_{gen}$ defines the entropy generation rate and T_0 is the temperature. In order to express equation 2 in terms of exergy destruction rate, the equation can be written as,

$$\dot{X}_{in} - \dot{X}_{out} - \dot{X}_{dest} = \dot{X}_{sys} \quad (3)$$

Where $\dot{X}_{dest}$ is exergy destruction rate (lost work potential) which provides a sagacious manner to compare lost available work across different scenarios, and can be defined as [11];

$$\dot{X}_{dest} = T_0 \, \dot{S}_{gen} \quad (4)$$

Equation 4 can alternatively be written as [11];

$$\dot{S}_{gen} = \frac{\dot{X}_{dest}}{T_0} \quad (5)$$

In this application the viscous dissipation rate Φ is the primary contributor to the entropy generation rate per unit volume [10], finally,

$$\dot{S}_{gen} = \frac{\dot{\Phi}}{T} \quad (6)$$

Entropy generation is one way to identify potential sources of reduced efficiency when comparing wingtip vortices. It provides a good metric to compare across many scenarios (different wings, wingtip shapes, Reynolds numbers etc.). The equation for the viscous dissipation rate [12] in the Trefftz plane can be written as;

$$\dot{\Phi} = \mu \left[2\left(\frac{\partial v}{\partial y}\right)^2 + 2\left(\frac{\partial w}{\partial z}\right)^2 + \left(\frac{\partial v}{\partial z} + \frac{\partial w}{\partial y}\right)^2 \right] + k \left[\left(\frac{\partial T}{\partial y}\right)^2 + \left(\frac{\partial T}{\partial z}\right)^2 \right] \quad (7)$$

where Φ is the viscous dissipation rate, v is the velocity component in the y direction, w is the velocity component in the z direction, μ is the dynamic viscosity and T is temperature. As mentioned in the previous section, the local temperature gradients were relatively small and therefore had negligible effect on the entropy generation. In concert with this assumption, equation (7) simplifies to;

$$\dot{\Phi} = \mu \left[2\left(\frac{\partial v}{\partial y}\right)^2 + 2\left(\frac{\partial w}{\partial z}\right)^2 + \left(\frac{\partial v}{\partial z} + \frac{\partial w}{\partial y}\right)^2 \right] \quad (8)$$

IV. Results

The total exergy, exergy distributions, and the means of exergy transport in a wingtip vortex were examined from 4° to 15° angle of attack. Each term (A, B and C) in the viscous dissipation rate equation (8) was plotted to understand its contribution. From the equation, it is noteworthy that the radial core growth, which is stretching (A and B), and skewing (C) contribute to exergy loss whereas pure axial rotation does not. Figure 4 shows the contribution of the stress terms as a function of angle of attack. A second order finite difference technique was used. Each of the three terms was compared to the total integrated exergy obtained. It was seen that the largest contribution per unit volume was achieved from the skewing term. Errors shown for each of the terms are several orders of magnitude less than the absolute values of exergy.

$$\Phi = \mu \left[\underbrace{2\left(\frac{\partial v}{\partial y}\right)^2}_{\mathbf{A}} + \underbrace{2\left(\frac{\partial w}{\partial z}\right)^2}_{\mathbf{B}} + \underbrace{\left(\frac{\partial v}{\partial z} + \frac{\partial w}{\partial y}\right)^2}_{\mathbf{C}} \right]$$

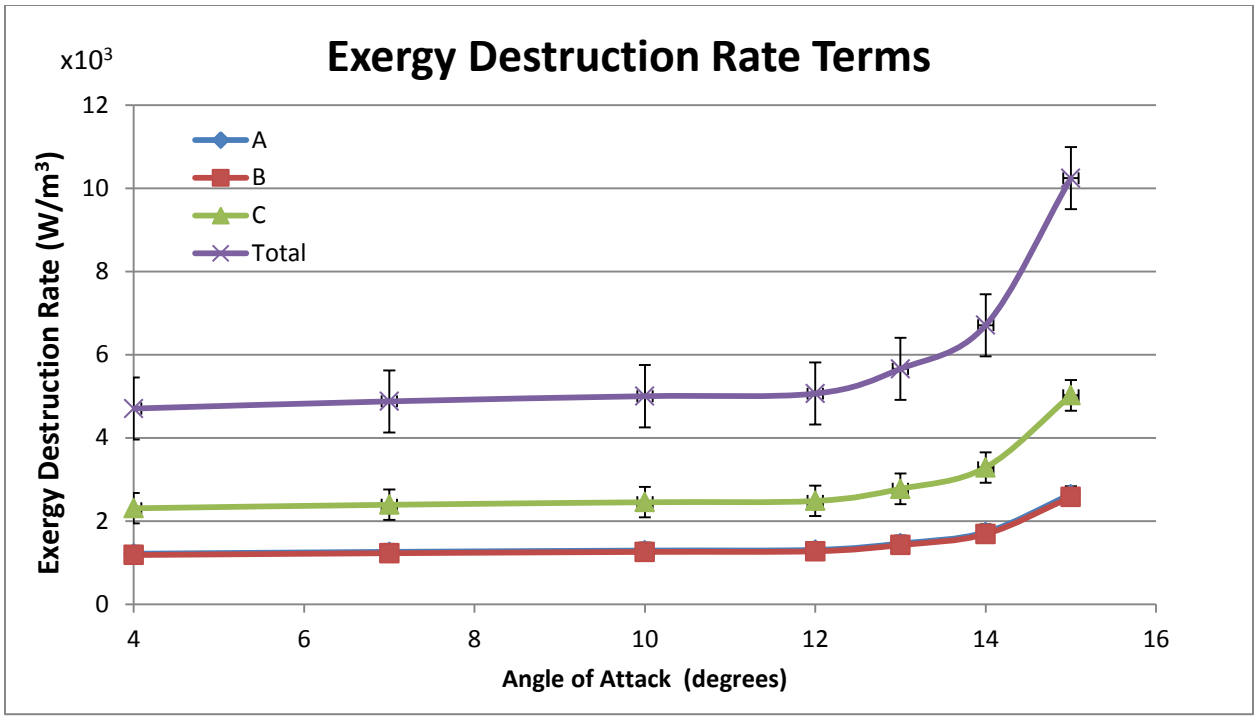

Fig. 4 Contribution from each term showing skewing (C) as most significant while stretching (A and B) demonstrates symmetry around the vortex.

In order to estimate the errors in the velocity gradient (exergy) terms shown in figure 4, the Kline-McClintock (K-M) Uncertainty method [13] was applied.

Applying the K-M method, the uncertainty in the absolute velocity is given by;

$$W_v = \sqrt{\left[\left(\frac{\partial v}{\partial x}\, w_x\right)^2 + \left(\frac{\partial v}{\partial t}\, w_t\right)^2\right]} \tag{10}$$

Where w_x is the spatial uncertainty of 0.16 pixel/pixel [14] and w_t is the temporal uncertainty of 5 ns. To calculate the uncertainty in the exergy terms, the velocity gradient from the viscous dissipation rate (eq. 8) can be expressed as being most dependent upon;

$$A = \mu\left[2\left(\frac{\partial v}{\partial y}\right)^2\right] \tag{11}$$

Subsequently, the uncertainty in the gradient (eq. 11) is calculated by;

$$W_A = \sqrt{\left[\left(\frac{\partial A}{\partial x}\, w_x\right)^2 + \left(\frac{\partial A}{\partial v}\, w_v\right)^2\right]} \qquad (12)$$

Where w_x is the uncertainty in the spatial distance and w_v is the uncertainty in the velocity. The error in the exergy terms is several orders of magnitude less than the absolute exergy value. The overall error is dominated by the uncertainty in the spatial term.

To provide a context for the factors influencing the exergy distribution, the normalized v and w velocity components were plotted as shown in Figures 5 and 6 respectively.

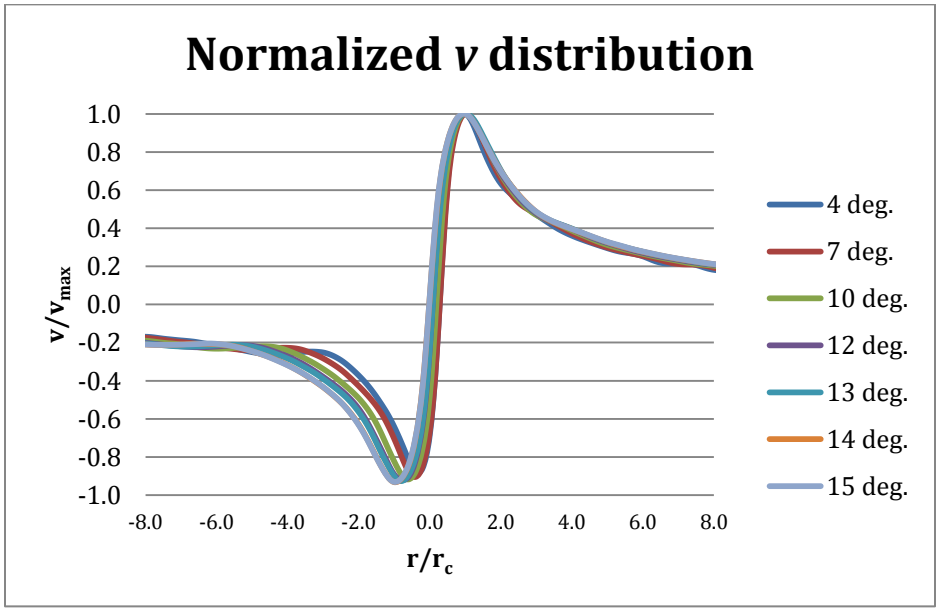

Fig. 5 Normalized v distribution showing similarity across the range of angles of attack.

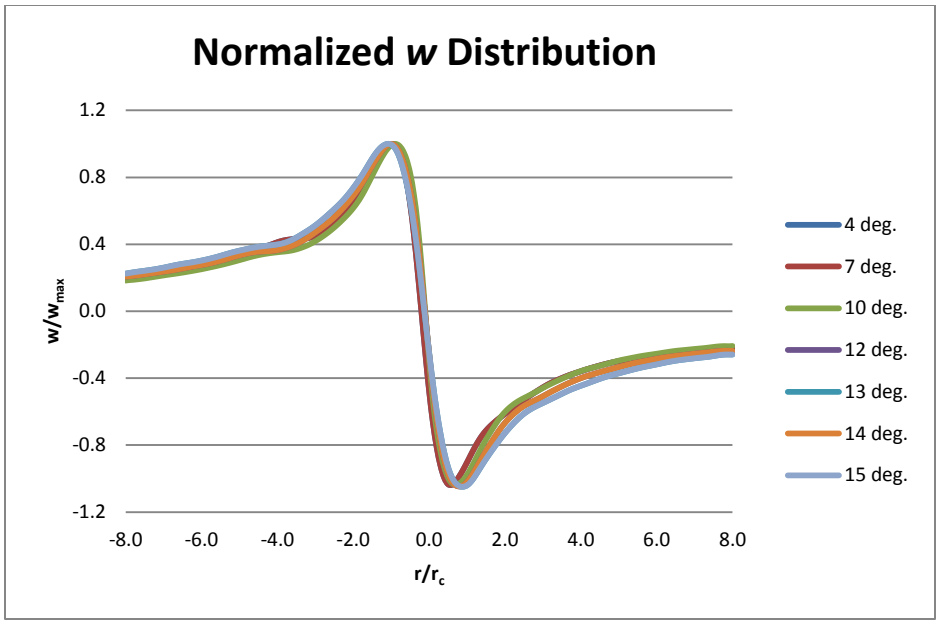

Fig. 6 Normalized w distribution showing similarity across the range of angles of attack.

Figures 5 and 6 show the distributions of normalized velocity components in the Trefftz plane. The *y*-direction velocity component distributions in Figure 5 are normalized by the maximum value for the associated angle of attack, $v^*=v/v_{max}$ and likewise for the *z*-direction velocity component (w), $w^*=w/w_{max}$ in Figure 6. The spatial axis in each of the two figures is normalized by the radius of the vortex core. In each of the two figures, the shaded region indicates the location of the boundary of the vortex inner core. These boundaries were determined from the peak tangential velocities for the given direction. For all angles of attack, dissimilarities can be observed in the normalized velocity distributions near the boundary of the inner core in an otherwise consistent distribution.

In order to calculate the circulation at each angle of attack, two separate methods of calculating circulation were used and compared. First, the area integral of the vorticity was calculated. As a first step, the vortex identification was accomplished by determining the vortex center (Γ_1) and vortex core boundary (Γ_2). These capital Greek letters Gamma are not to be confused with the circulation. Graftieaux et al. [15] derived the scalar functions (Γ_1 and Γ_2) to characterize the locations of center and boundary of the vortex, by considering the topology of the velocity field. The scalar functions for Γ_1 and Γ_2 at a fixed point (P) in the measurement domain are shown in equations 13 and 14 respectively [15].

$$\Gamma_1(\mathrm{P}) = \frac{1}{S}\int_{M\epsilon S} \frac{(\mathrm{PM}\,\Lambda\, U_M)\,\mathrm{z}}{\|\mathrm{PM}\|.\|U_M\|}\,\mathrm{dS} = \frac{1}{S}\int_S \sin(\theta_M)\,\mathrm{d}S \qquad (13)$$

where S is a two dimensional area surrounding P, M lies in S and z is the unit vector normal to the measurement plane; θ_M represents the angle between the velocity vector U_M and the radius vector PM; Γ_1 is a dimensionless scalar, with $|\Gamma_1|$ bounded by 1. The equation for Γ_2 is derived by equation 4 and takes into account a local convection velocity U_P around P where $U_P = \frac{1}{S}\int_S U\,\mathrm{d}S$ [15].

$$\Gamma_2(\mathrm{P}) = \frac{1}{S}\int_{M\epsilon S} \frac{[\mathrm{PM}\,\Lambda\,(U_M - \tilde{U}_P]\,\mathrm{z}}{\|\mathrm{PM}\|.\|U_M - \tilde{U}_P\|}\,\mathrm{d}S \qquad (14)$$

The authors suggested that, based on the local maximum detection, the vortex center (Γ_1) values typically range from 0.9 to 1. Conversely, the vortex core (Γ_2), depending on the rotation, is typically in the range 0.6 to 0.7. The initial baseline value of Γ_1 and Γ_2 was assumed to be 0.93 and 0.63. A sensitivity analysis was performed on the circulation values by varying the Γ_1 and Γ_2 values over the respective cited ranges. Sensitivity analysis was performed to examine if there is a change in the profiles.

As a second method, circulation was calculated from the Stokes theorem as the line integral of velocity. Application of circulation obtained from Stokes Method relies on the presence of an irrotational region surrounding the core. Circulation, determined as the line integral of velocity, calculated through;

$$\Gamma_{Stokes} = 2\pi v r$$

Circulation determined by invoking Stokes theorem predicts that for a circular core flow the circulation remains constant. As can be clearly seen in Figure 7, however the circulation calculated in this manner varies across an unacceptably wide range as a function of vortex radius. Whilst this exercise provides a measure of circulation calculated from a more-conventional method, it is not considered suitably robust in this application. As a result of this somewhat ambiguous determination of circulation, a more robust method was employed that has found great favor in vortex identification circles.

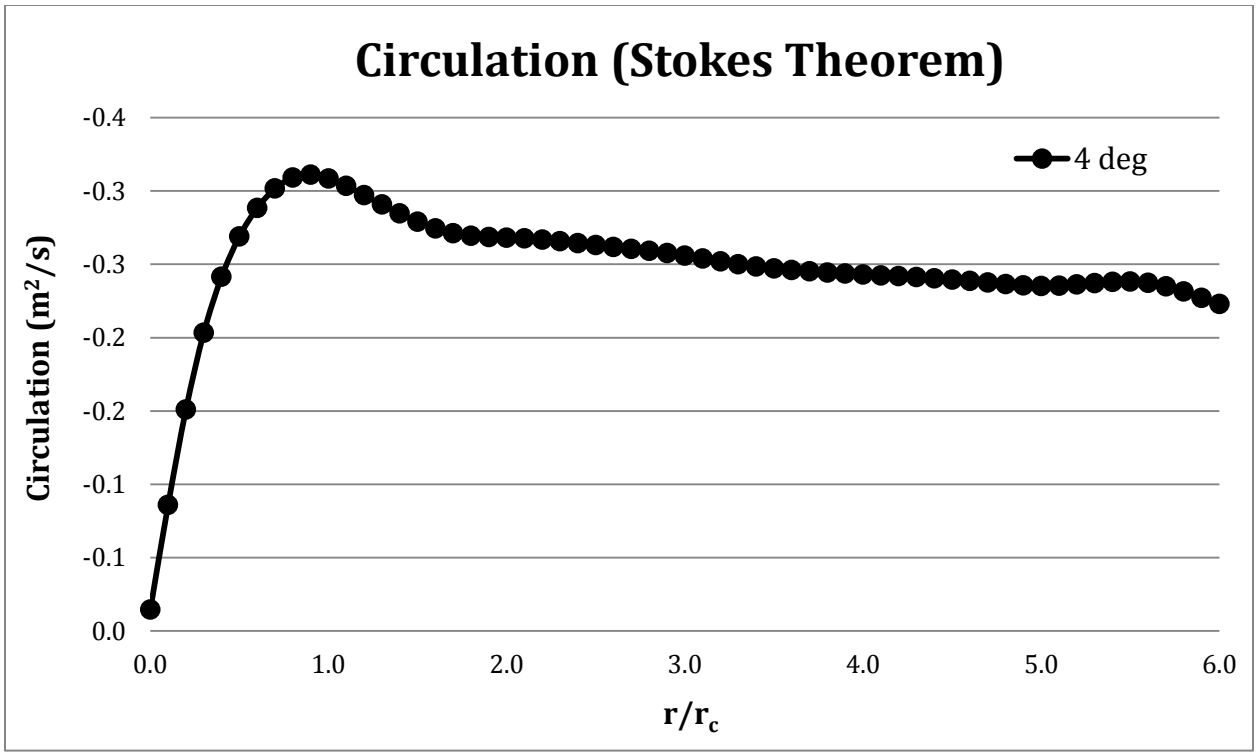

Fig. 7 Circulation (obtained from the Stokes method) for 4 degree alpha showing continuous variations in magnitude of circulation as a function of vortex radius even in the region surrounding the core.

Calculation of circulation using Stokes' theorem shows similarity in the trends irrespective of the radial location relative to the vortex core the tangential velocity is sampled from. Unfortunately, though, the value of circulation was sensitive to the choice of radial location regardless of the region sampled and more robust and repeatable methods were employed to determine the circulation. Figure 8 shows the comparison of circulation obtained from both methods as well as the sensitivity analysis as a function of angle of attack. The graph shows sensitivity with Γ_1 at 0.87, 0.9, 0.96 and 0.99 and Γ_2 at 0.57, 0.63, 0.66, and 0.69 relative to the baseline values, t. The most important characteristic to note is that regardless of the definition of the vortex center or boundary used, the trends remain same with decay present in circulation from 14° to 15°. While the circulation obtained from the line integral method differs slightly but was obtained on the same order of magnitude as expected.

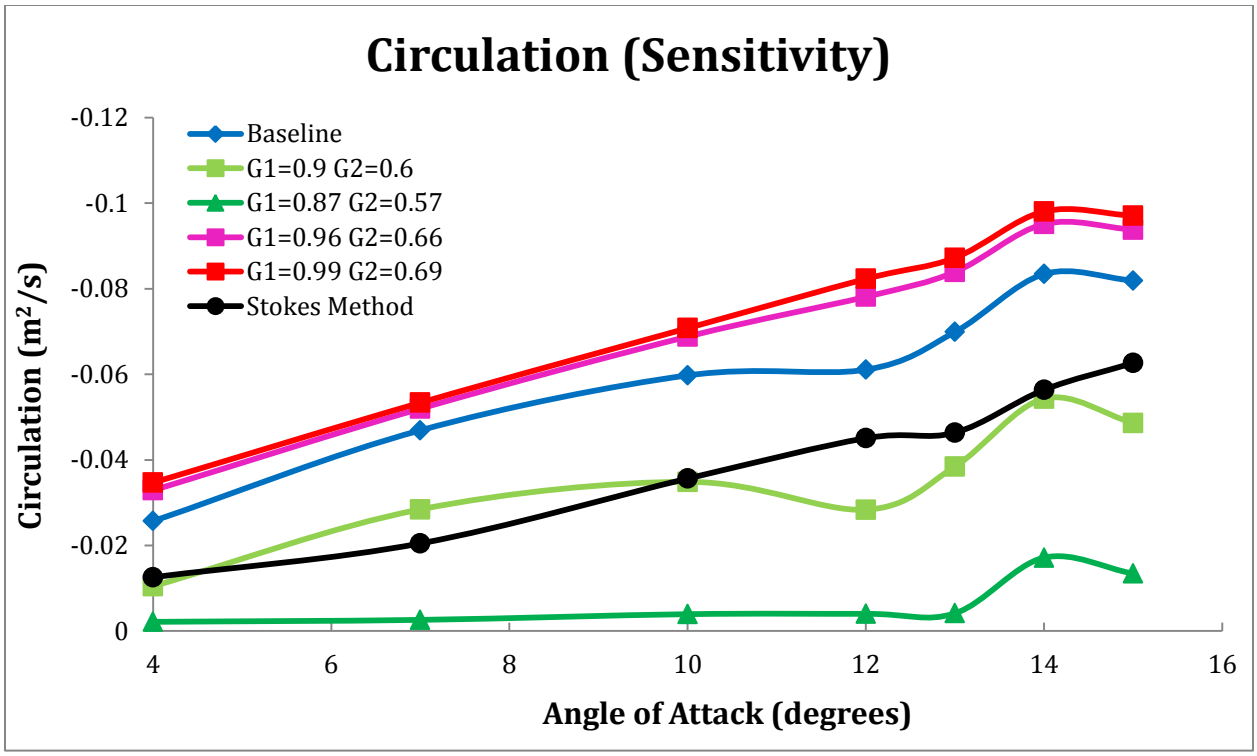

Fig. 8 Comparison of circulation determined from the area integral method and the Stokes method. Sensitivity analysis of circulation showing similarity in the trends irrespective of the vortex core radius.

In an effort to better characterize the nature of the changes in the vortex topology, a number of traditional vortex radial circulation distribution models were employed. It was hoped that any deviations from the traditional models would better isolate possible sources for any differences in predicted behavior.

The circulation was normalized on the basis of the viscous inner core for each angle of attack. The values for the Γ_1 and Γ_2 were used as 0.93 and 0.63 respectively. Birch [16] compared a number of models; Hoffman and Joubert [17], Phillips [18] and Batchelor [19], to reveal universal inner-scaled circulation profiles. The calculated circulation was normalized by its inner core radius where the boundary of the inner core was defined by the location of the maximum velocity tangential to the vortex rotation. Equations 15-17 represent the models found in the literature, where Γ is the circulation, $\eta = r/r_c$ is the non-dimensional radial coordinate, and r_c and Γ_c are the vortex core radius and core circulation, respectively [16].

Hoffman-Joubert Model [17]

$$\frac{\Gamma(\eta)}{\Gamma_c} = A_0\eta^2 \qquad 0 \le \eta \lesssim 0.4,$$

$$\frac{\Gamma(\eta)}{\Gamma_c} = 1 + A_1 \ln(\eta) \qquad 0.5 \lesssim \eta \lesssim 1.4,$$

A0 = 1.83
A1 = 0.929

(15)

Phillips Model [18] $$\frac{\Gamma(\eta)}{\Gamma_c} = \sum_{k=1}^{n} B_k \eta^{2k}, \qquad 0 \le \eta \lesssim 1.3,$$ B1 = 1.7720 B2 = -1.0467 B3 = 0.2747 (16)

Batchelor Model [19] $$\frac{\Gamma(\eta)}{\Gamma_c} = \frac{1 - \exp(-\alpha\eta^2)}{1 - \exp(-\alpha)},$$ α = 1.26543 (17)

Figures 9, 10 and 11 show the normalized circulation profiles for three different groupings of angle of attack:

1. 4º and 7º,
2. 10º, 11º and 12º, and
3. 14º and 15º

The experimentally determined profiles are compared to several theoretical models found in the literature. In Figure 9, the change in the profiles from 4º to 7º is intriguing. The 4º curve deviates slightly from the models with a concave profile while at 7º a convex profile can be seen. This implies that the core circulation and hence the lift is less at 4º when compared to the 7º case. This change is thought to be related to the transition from a wake-like to a jet-like wingtip vortex axial core flow profile. In some sense, a difference in behavior between these two angles of attack was expected. The curves in Figure 10 show convex profiles with the distribution of circulation remaining along the path of that observed from the cited models. Significant deviation is seen in Figure 11 with the convex profiles for both the 14 º and 15 º cases. At present there is no obvious explanation for this change in behavior. It was perhaps once again possible to anticipate this result given the change in integrated circulation seen above in Figure 8. This difference should motivate further research in an effort to explore cases involving higher angles of attack.

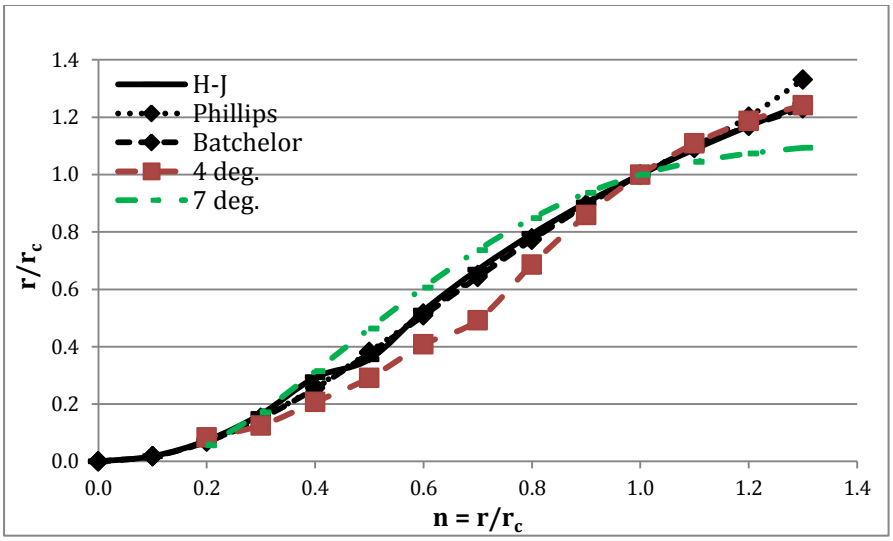

Fig. 9 Comparison of normalized circulation profiles with theoretical models showing deviation from concave (4º) to convex profile (7º)

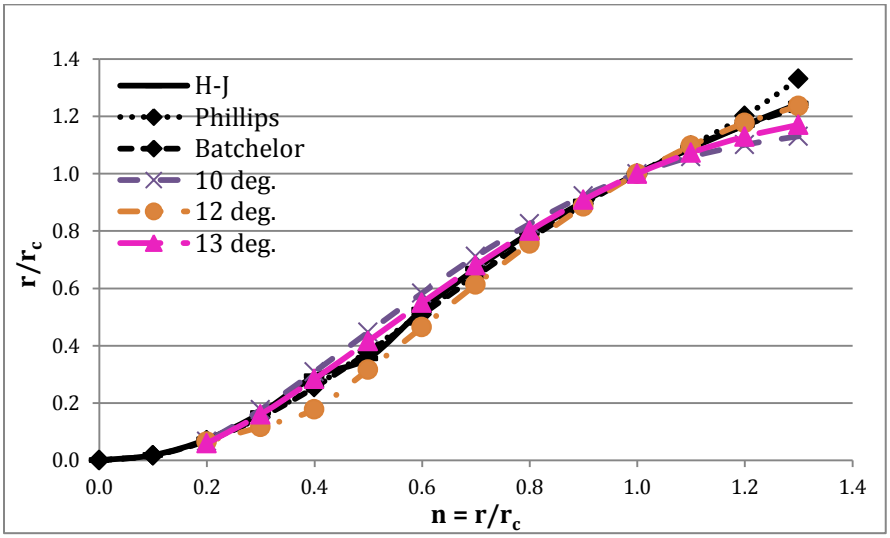

Fig. 10 Comparison of normalized circulation profiles with theoretical models showing consistency of the convex profiles

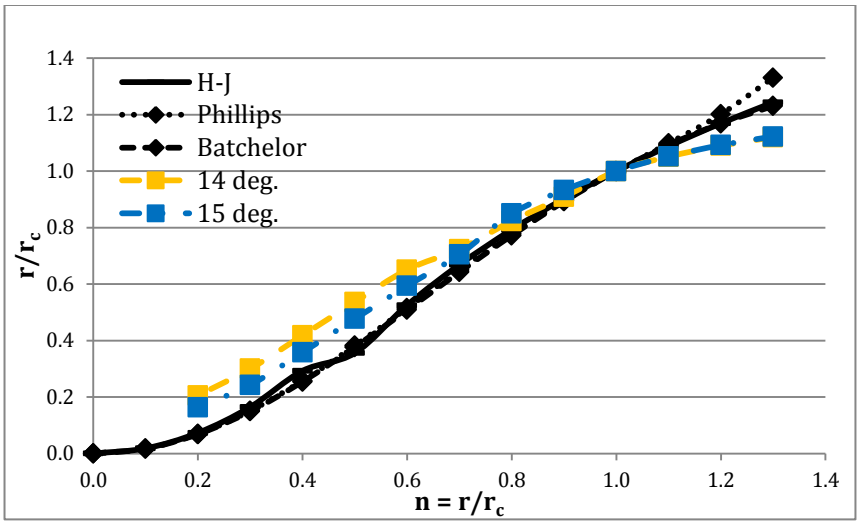

Fig. 11 Comparison of normalized circulation profiles with theoretical models showing significant deviation (from 14º to 15º).

The most significant outcome from comparing circulation profiles with accepted profile models from the literature lies in the change in shape of the curve from concave (at 4º) to weakly convex (at 7º) which happens to correspond to the region in which the axial core flow crossover from jet-like to wake-like behavior occurs. It is intriguing that the profiles continue to exhibit a convex shape at higher angles of attack. This emphasizes the point that there is a change in the nature of the profile after the crossover point as expected.

Transitioning from the vortex core circulation behavior, the focus will now be placed on the out of plane component and correlating the behavior of derivative quantities to these changes. Figure 12 shows the x-direction velocity (core axial flow) distribution for each angle of attack. A distinct change in behavior can be seen in the distribution. The switch from wake-like to jet-like out of plane velocity profile from 4° to7º angle of attack, as described in [7], is noteworthy. This profile switch coincides with the crossover point in the exergy versus the maximum lift-to-drag ratio plot in Figure 13. The L/D ratio was obtained from XFoil for the Clark-Y airfoil under the same conditions as the experiment. The L/D data obtained from XFoil was extended to three-dimensions via the Helmbold equation [20]

$$\frac{C_L}{\alpha} = \frac{a_0}{\sqrt{\left\{1+\left(\frac{a_0}{\pi AR}\right)^2\right\}}+\frac{a_0}{\pi AR}} \tag{14}$$

Where C_L is the three dimensional coefficient of lift, α is the angle of attack, a_0 is the effective angle of attack and AR is the aspect ratio of the wing. The XFoil results were restricted to the angles of attack for which the experimental cross-stream data was obtained. The L/D increases in the range from 4° to 7° before reaching a plateau at approximately 8° angle of attack. The significance of the L/D curve for Clark-Y airfoil presented here lies in the general trends and not the absolute values.

It is important to note that the peak could be anywhere in the range from 5° to 6° angle of attack, which would coincide with the axial switchover between 4° and 7° angle of attack. This transition corresponds to the switchover from a wake-like (at 4°) core axial flow profile to a jet-like profile (at 7°). This aforementioned switchover is manifested in a profile cut of axial velocity through the vortex in Figure 12 at 4° and 7° as well as for the remaining angles of attack tested.

Integrated total exergy destruction in the vortex (Figure 13) was calculated by area integration. The exergy destruction rate changes slightly up to 12° degrees until the slope increases significantly between 12° and 13° angle of attack. In the range from 13° to 15° there is a substantial increase in the slope of the integrated exergy curve. Correspondingly, there is a large drop in aerodynamic efficiency from 12° to 14° angle of attack after which the ratio settles down. Thus, the change in macroscopic integrated total exergy shows little indication of the switchover condition at maximum L/D. However, it does appear to capture the changes in performance at the higher angles of attack.

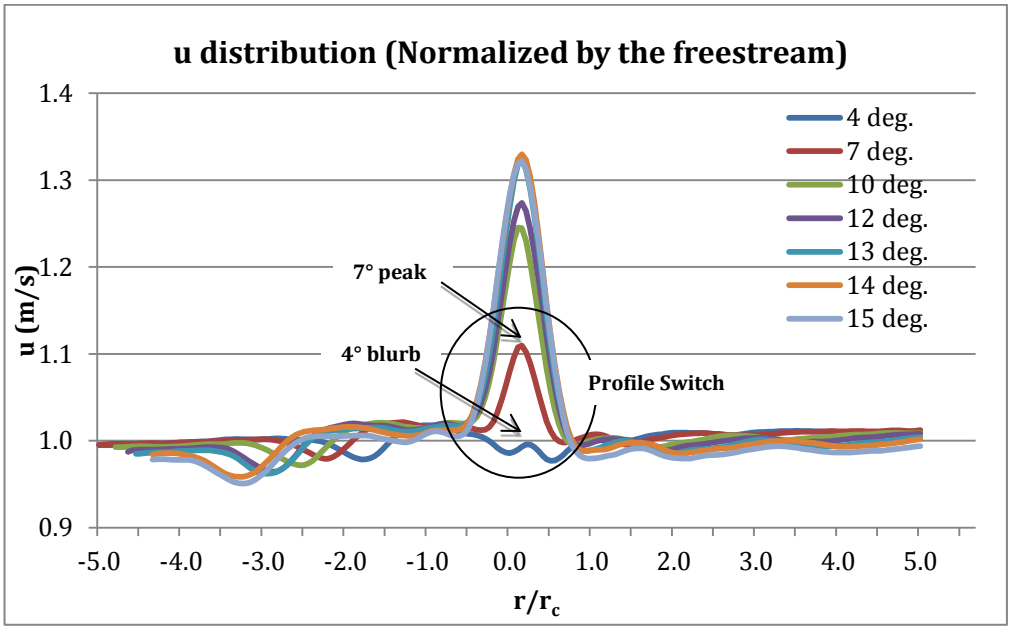

Fig. 12 *u* distribution shows a distinct difference with a switch-over from wake like (4°) to jet like (7°) profile.

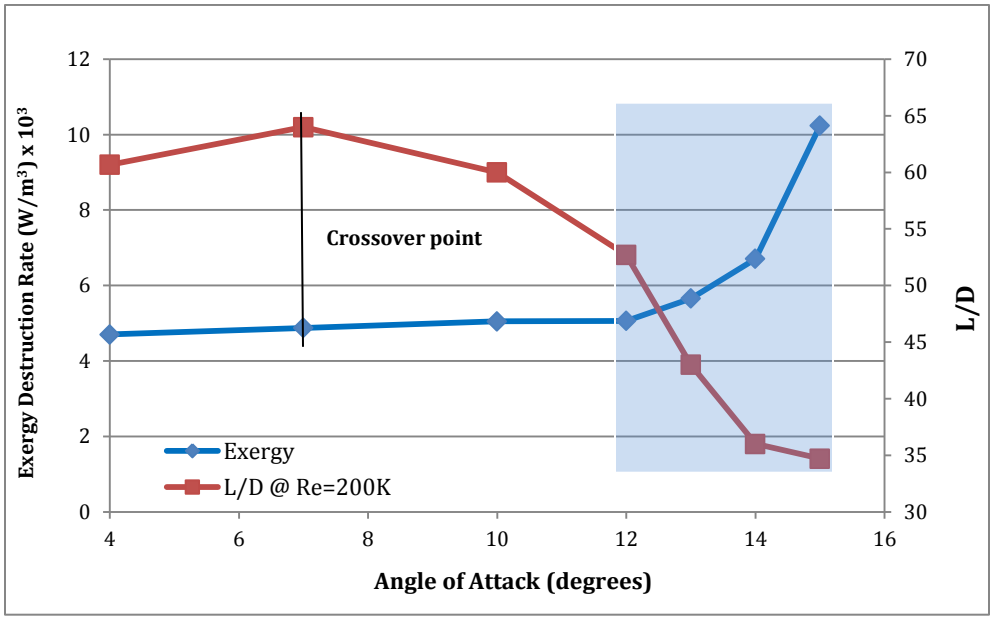

Fig. 13 Integrated total exergy and L/D showing steady increase before a crossover point at 7°. The shaded area emphasizes the region of significant changes

Greater insight into the behavior of the vorticity and exergy distributions can be gained from Figures 14 and 15 respectively. Figure 14 shows the vorticity distribution across all angles of attack tested. There is no difference in the general shape of the profiles. Immediately noticeable, however, is the grouping of the 12° and 13° cases and separately, the 14° and 15° cases. Referring back to the total exergy plotted in Figure 13 above, it is noted that the exergy also experienced a large increment in slope around these two pairs of angle of attack as well.

The profiles through the wingtip vortices of absolute exergy as a function of angle of attack are shown in Figure 15. Similar to the vorticity profiles, the exergy profiles also group at 12° and 13° and 14° and 15° as would be expected from the total exergy results from Figure 13. It is important to notice that these two groups of most similar vorticity and absolute exergy distribution demonstrate overlapping of the results at high angles of attack. From the integrated total exergy variation with angle of attack in Figure 13, it is perhaps unsurprising that the exergy distributions are clustered at 12° and 13°, and again around 14° and 15°. The clustering of the profiles is clearly visible in the overall trend in Figure 15. This behavior is most likely related to changing vortex topology at the wing-tip. The results for the square edge tip maintains lift at high angles of attack resulting from small regions of

concentrated vorticity that remain attached to the sharp corners in combination with massive downwash over the wing. This serves to keep the flow attached to the wing's upper surface longer than with other wingtip shapes tested and published elsewhere.

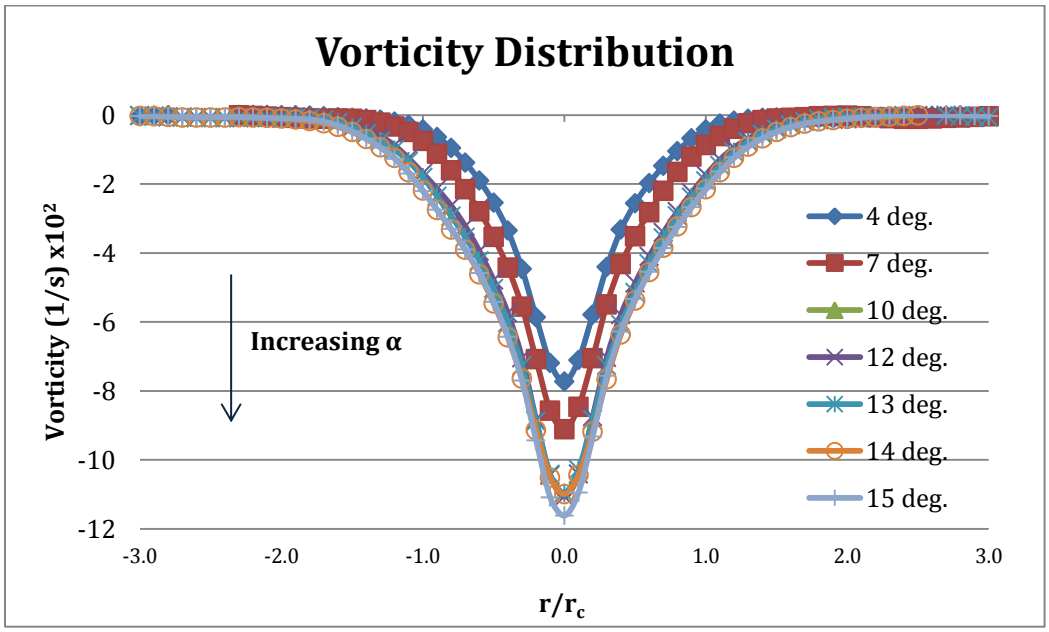

Fig. 14 Vorticity distribution shows groupings at 11° and 12° and at 14° and 15°

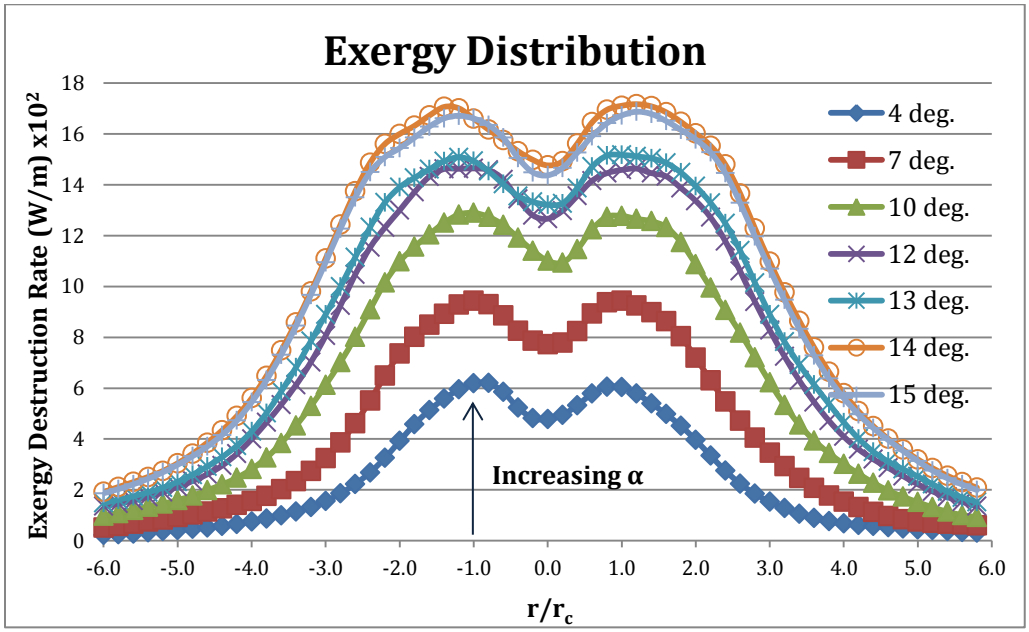

Fig. 15 Exergy distribution shows profile groupings at 12° and 13° and at 14° and 15°

The normalized vorticity and exergy distributions are shown in Figures 16 and 17 respectively as a function of angle of attack. The plot of normalized vorticity shows no significant change in overall shape regardless of the angle of attack. The interpretation of the exergy distributions across the vortices as a function of angle of attack becomes intriguing since angles of attack 10° through 15° exhibit essentially the same distribution of exergy across the vortices. However, between 4° and 7° angle of attack [collectively] and the remainder of the cases evaluated, there is a palpable difference in the exergy distributions across the viscous inner core of the vortex. This difference in exergy distribution coincides with the crossover point (from wake-like to jet-like in the axial flow/out of plane vortex core velocity) discussed earlier, indicating the attainment of the maximum lift to drag ratio angle of attack. Thus, despite the fact that the macroscopic evaluation of total integrated exergy was unable to identify these changes, the actual profile of the distribution of normalized exergy very clearly indicates this transition phase and likely merits further inquiry.

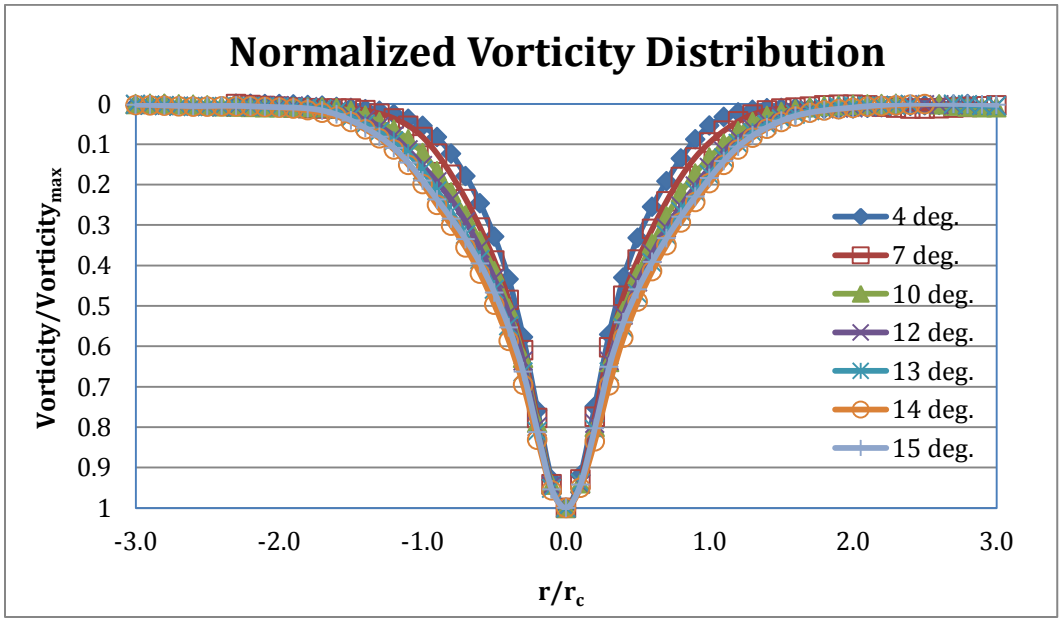

Fig. 16 Vorticity normalized by its maximum value shows coincident behavior.

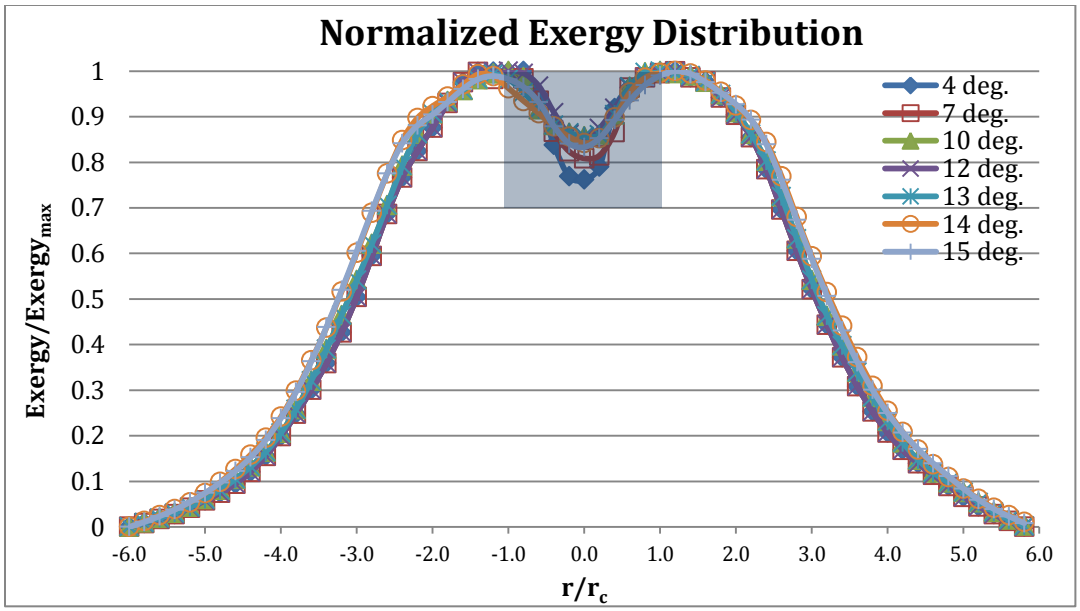

Fig. 17 Normalized exergy distribution shows divergent behavior at the crossover. Shaded area indicates the vortex core location.

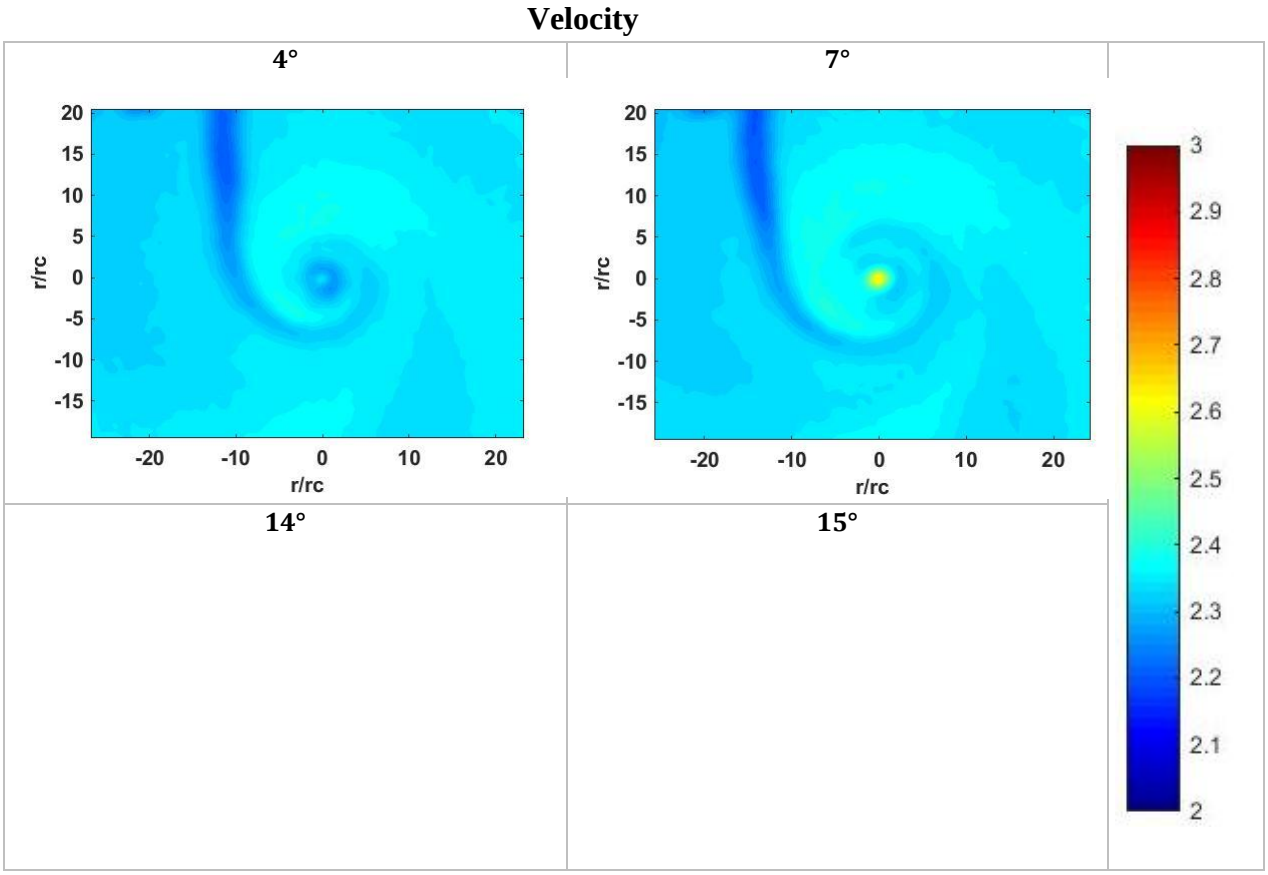

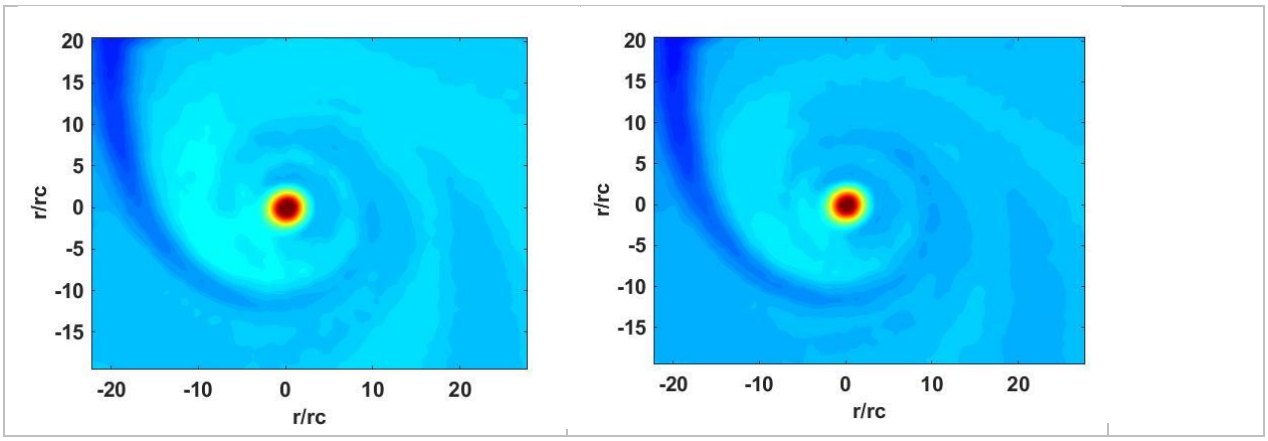

Fig. 18 Velocity contours comparison for various angles of attack showing visible difference in integrated magnitude.

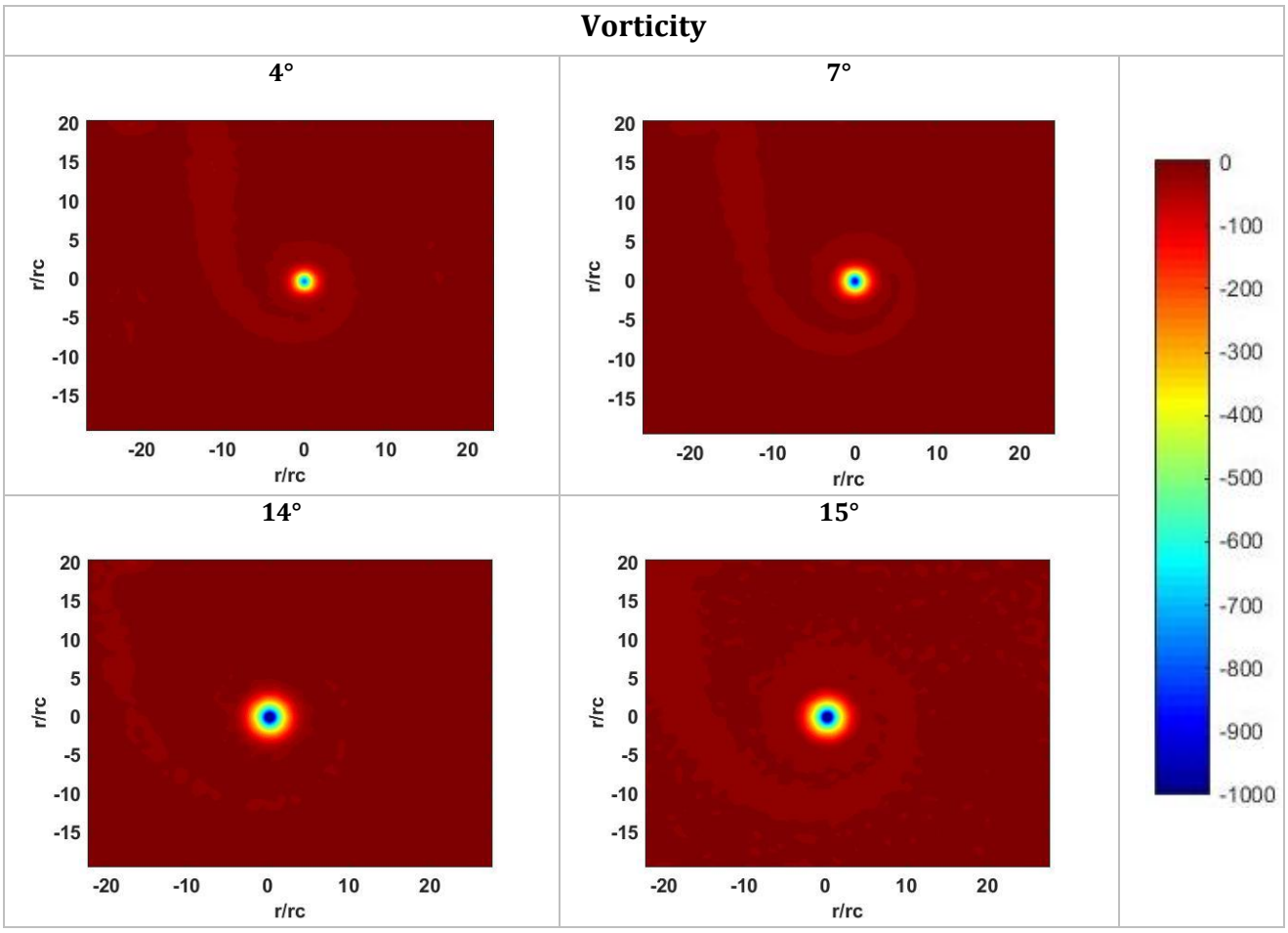

Fig. 19 Vorticity contours comparison contours for various angles of attack showing visible difference in integrated magnitude.

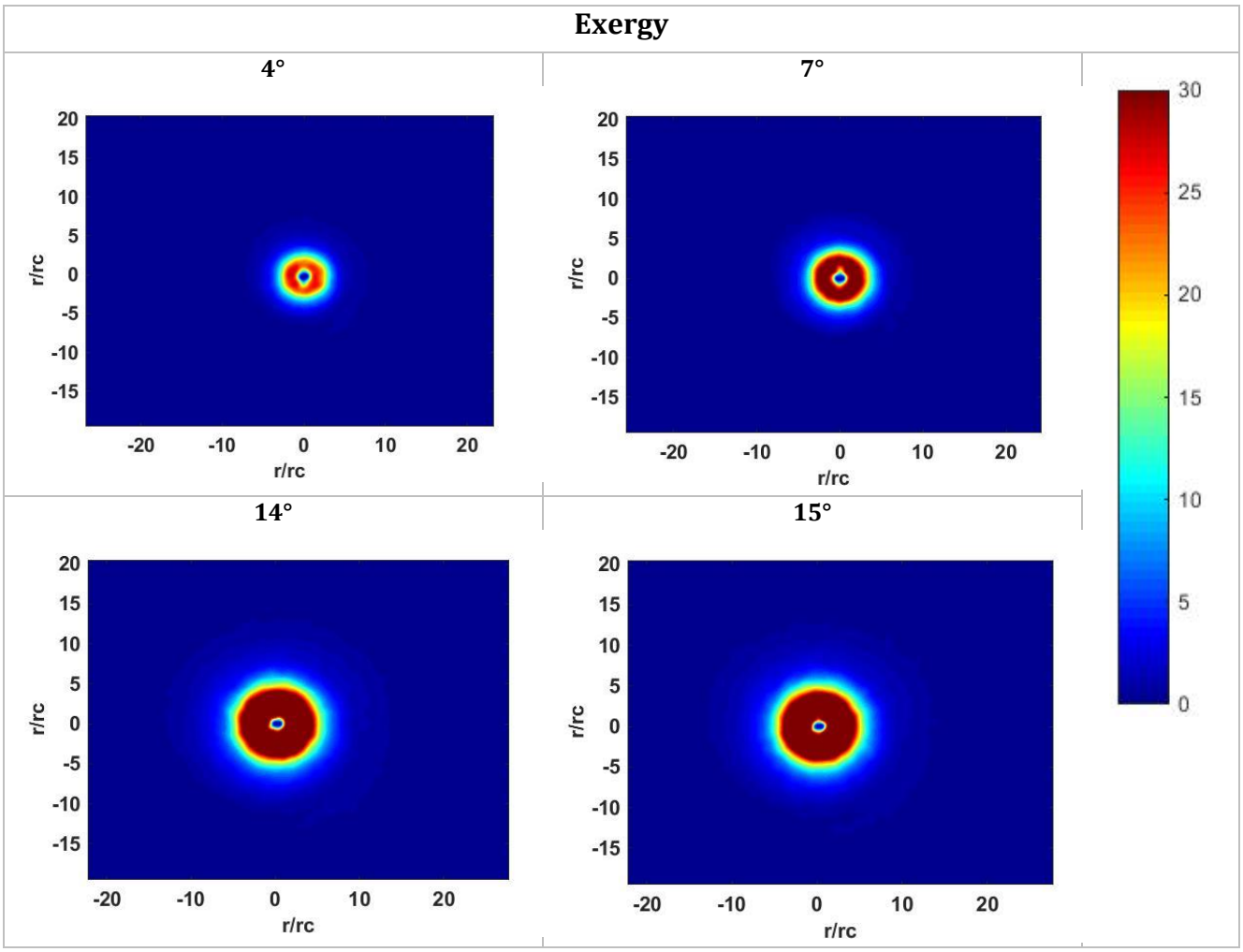

Fig. 20 Exergy contours comparison contours for various angles of attack showing visible difference in integrated magnitude.

Figures 18, 19 and 20 show the velocity, vorticity and exergy contour distribution for various angle of attack cases respectively. Several lower and higher angles of attack cases are shown to virtually visualize the flow for each of the calculated components. Continuous distribution of the growth in the viscous inner core in the vorticity and exergy contours can be seen. Various contours show the visual representation of wake-like profile (at 4° and 7°) as well as the jet-like profile (at 14° and 15°) angles of attack. The figures highlight the similarities and differences within these two different regions. The first case (4°) indicates wake like profile which can be compared across other cases at increasing angles of attack. Comparing the u velocity contours, there is a distinct difference. There is no distinction or definition in the core at 4° angle of attack. The defined core seen at the other angles of attack can be seen as an indication of a jet like profile. Across the vorticity contours, a clear increase in the radial

distribution of vorticity can be observed through the core of the vortex. This was previously visualized in the difference between the 4° and 7° cases in Figure 14. Figure 17 shows a slice through the spatially normalized distribution which demonstrates growth in the inner core region (shaded region indicates the approximate boundary of the inner core). Most notably, between 4° and 7° there is a substantial change in the absolute inner core exergy contour. What is even more surprising is that the out of plane change in axial core behavior from wake-like to jet-like is identified via the exergy profile. This out of plane change is not identified by any of the other parameters more traditionally used to evaluate wingtip vortex characteristics.

What is most intriguing about this result is that although only 2-d Trefftz plane data was used to obtain the exergy distribution across the plane of the wingtip vortices, the crossover point for the out of plane change from wake-like to jet-like core axial flow (which corresponds to the attainment of the maximum lift to drag ratio angle of attack) can be identified by the *in*-plane exergy distribution. This result has potential implications for the reduction of lift induced drag through manipulation of the wingtip vortex formation and dissipation processes. Exergy distribution can be used as an indicator of overall integrated wing performance or as an indicator of the manner in which a wingtip vortex would dissipate under a given set of conditions.

IV. Conclusions

In this paper, an exergy-based technique is established to explore the work potential of the wingtip vortex as a function of angle of attack. Several wingtip vortex characteristics are explored through this approach. The exergy-based analysis has a significant advantage over traditional approaches as a method for system design because it provides detailed information as to how the design is driven towards the optimum performance. The wingtip vortex near-wake exergy was calculated from experimental velocity field data as a function of angle of attack. The increase at maximum lift-to-drag ratio from 4° to 7° angle of attack showed a transition from wake-like (at 4°) to jet-like vortex core axial flow profile (at 7°). The exergy-based technique was able to identify the change in the out of plane profile (at the crossover point between wake-like and jet-like profile). Through the exergy-based technique, distinct changes in the L/D performance were accurately identified. The interpretation of these profiles would not be possible with a conventional energy based approach.

Additionally, the macroscopic integrated total exergy reflected changes in lift performance at the higher angles of attack meriting further research and application to other wings/airfoils. Looking at the wingtip vortex

through the lens of exergy-based methods has been beneficial in this case, and if extended could potentially be employed in producing more efficient wingtips. As a future investigation in the exergy-based approach, conventional airfoils with known specifications/behavior across a broader array of conditions could be used. In addition, the increment in the angle of attack would be reduced to better highlight the physics behind some of the transitions identified in the present results. More specifically, a reduction in the increment in angle of attack in the vicinity of the cross-over point (Max L/D point) could yield greater insight into the mechanisms responsible for such a cross-over. This understanding could be used to improve the performance of the airplane in off-design cruise conditions. Lower Reynolds number and higher angle of attack would also be expected to reveal interesting results.

References

[1] Alabi, K., Spakovskyρ, M.V., Ladeinde, L., Moorhouse, D., Camberos, J. A., et al., "A comparison of empirical and CFD-based exergy modelling for the airframe subsystem of aircraft design," *25th International congress of the aeronautical sciences* 2006.

[2] Schlichting, H., and Truckenbrodt, E., Aerodynamik des Flugzeugs. Zweiter Band. 2.Aufl. Berlin, Heidelberg, New York: Springer-Verlag; 1967.

[3] Breitsamter, C., "Wake vortex characteristics of transport aircraft," *Progress in Aerospace Sciences* 47 (2011) 89–134.

[4] Li, H., Stewart, J., Figliola, R. S., "Exergy based design methodology for Airfoil shape optimization and wing analysis," *25th international congress of the aeronautical sciences* 2006.

[5] Doty, J. H., Camberos, J. A., and Moorhouse, D. J., "Benefits of Exergy-Based Analysis for Aerospace Engineering Applications," *AIAA Journal*, 2008 pp. 4355.

[6] Figliola, R. and Tipton, R., "An Exergy-Based Methodology for Decision-Based Design of Integrated Aircraft Thermal Systems," *SAE Technical Paper* 2000-01-5527, 2000, doi:10.4271/2000-01-5527.

[7] Lee, T., and Pereira, J., "Nature of Wakelike and Jetlike Axial Tip Vortex Flows," *Journal of Aircraft*, Vol. 47, No. 6, November–December 2010.

[8] Institute of Aeronautics and Astronautics, RWTH Aachen University, Wullnerstr. 7, 52062 Aachen, Germany, http://www.ilr.rwth-aachen.de.

[9] Buffo R. M., Wolf C. C., Dufhaus,S., Hoernschemeyer, R., Stumpf, E., "Vortex Creation and Wing-Tip Geometry Dependencies", 30th AIAA Applied Aerodynamics Conference 25 - 28 June 2012, New Orleans, Louisiana

[10] A. Bejan, Entropy Generation Minimization, CRC Press LLC, Boca Raton, FL ©1996

[11] Y. A. Cengel & M. A. Boles, Thermodynamics An Engineering Approach 4th Edition, McGrawHill Companies, Inc., New York, NY ©2002.

[12] F. M. White, Viscous Fluid Flow 3rd Edition, McGraw-Hill Companies, Inc., New York, NY ©2006.

[13] S. J. Kline and F. A. McClintock, Describing Uncertainties in Single-Sample Experiments", Mechanical Engineering, pg. 3, January 1953.

[14] Raffel M., WIllert C., Wereley S., Kompenhans J., Particle Image Velocimetry – A Practical Guide 2nd Edition, Springer Heidelberg New York, NY 2007.

[15] Graftieaux, L., Michard, M., and Grosjean, N., "Combining PIV, POD and Vortex Identification algorithms for the study of Unsteady Turbulent Swirling Flows," *Measurement Science and Technology*, Vol. 12, 2001, pp. 1422-1429.

[16] Birch, D. M., "Self-similarity of trailing vortices," *Physics of Fluids,* Vol. 24, No. 025105, 2012.; doi: 10.1063/1.3689179.

[17] Hoffman E. R., and Joubert, P. N., "Turbulent line vortices," *Journal of Fluid Mechanics*, Vol. 16, No. 395, 1963.

[18] Phillips, R. C., "The turbulent trailing vortex during roll-up," *Journal of Fluid Mechanics*, Vol. 105, No. 451, 1981.

[19] Batchelor, G. K., "Axial flow in trailing line vortices," *Journal of Fluid Mechanics*, Vol. 20, No. 645, 1964.

[20] H. B. Helmbold, Der unverwundene Ellipsenflfigel als tragellde Flache. Jahrb. 1942 d. Deutschen L Uftf Ahrtforschung.